UNIVERSITY OF COPENHAGEN
FACULTY OF SCIENCE

Sensitivity to Friction Changes: the Case of an Idealized Gullmarn Fjord

Floriane Océane Sudre

Submitted on the 18th, June 2019

Supervisor
Professor Markus Jochum, Physics of Ice, Climate and Earth, Niels Bohr Institute, University of Copenhagen

Co-supervisor
Professor Herbert Formayer, Institut für Meteorologie, University of Natural Resources and Life Science, Vienna

Abstract

The ocean is a vital component of the Earth's climate. As such, the ocean can also act as a powerful climate metric for global climate changes. Nonetheless, how accurately ocean properties and ocean circulation can be assessed by existing modelling is still source of debates and subject of numerous research projects. The present Thesis aims to contribute to such debates by better understanding the role of friction. It does so through a modelled study of water circulation in a selected Swedish fjord.

Although they are often neglected or roughly parametrized in large scale ocean models, bottom, vertical, and lateral friction might have a non negligible impact on ocean circulation. For the scope of the present Thesis, the influence of changes in bottom friction, vertical eddy viscosity, and lateral eddy viscosity parametrization are considered independently of each other. To clearly identify the role of those processes, this work relies upon the General Estuarine Transport Model (GETM) as applied to an idealized fjord, which has been modelled on the approximate dimensions of the Swedish Gullmarn fjord.

On the basis of these experiments, the Thesis suggests that the idealized fjord circulation is most sensitive to horizontal viscosity variations especially at the eastern boundary. In turn, variations in bottom and vertical frictions are found to be less significant. Additionally, the horizontal eddy viscosity pattern is found to resemble salinity distribution more than the velocity distribution, suggesting that the forced tidal flow has less impact on the idealized fjord circulation than the density fluctuation.

This work is part of a preliminary study for an observational expedition taking place in the Swedish Gullmarn fjord. The main objective of this broader project consists in testing the validity of assumptions on friction in ocean models. Within such context, the present work brings evidences that more research needs to be done to enquire the role of friction on the estuarine circulation, especially the horizontal eddy viscosity. It further provides the basis for the design of a more realistic model of the Gullmarn fjord.

Acknowledgment

I certainly felt overwhelmingly fortunate and immensely grateful while writing this thesis. It would be fair to start thanking the panel of the EnvEuro program for offering me the opportunity to deepen my education on environmental topics and climate science. Without them, I would not have been able to meet Herbert Formayer, co-supervisor of this thesis, and Markus Jochum, main supervisor, whose passion for oceanography is only a match to his eagerness in teaching and to his tendencies to humoristically confuse students. Without Markus, I would not have met Xaver whose kindness and patience were like glue to bind pieces of this project together. I also wish to thank Roman for taking care of Ægir, and Mads for lending me his copy of Pedlosky's *Ocean Circulation Theory*. I am most grateful to Falk, for friendly chats when they were most needed, and for the sharpest review of this thesis. Finally, without Luca, there would be no such thing as a thesis at all, and no sense of drama either.

Contents

1. Introduction

1.1 Motivation and relevance

As a central component of the Earth's climate, the oceans can act as a powerful climate indicator for global climate changes (Goosse 2015). Despite their crucial role in our climate system, oceans are still vastly unknown. Unsurprisingly, the accuracy of ocean models is still at the core of many research projects. The present Thesis aims to offer a contribution to the better understanding of the role of friction in the oceans. It does so through a case study focusing on the Swedish fjord of Gullmarn.

Although often neglected or approximately parametrized to ease the calculations when running large scale ocean models, friction might have a non-negligible impact on ocean circulation (Pedlosky 1996). Jochum et al. demonstrated how lateral eddy viscosity can affect the accuracy of ocean models (Jochum 2008); in a similar fashion, Guillou et al. explored the ocean circulation sensitivity to bottom roughness (Guillou 2013). Separately, Hibiya et al. highlighted the need for improving parametrisation of vertical mixing over rough bathymetry (Hibiya 2017).

One main reason behind weak parametrization or neglecting of small scale dissipation of unresolved motions might be related to the difficulty in explaining dissipation, both qualitatively and quantitatively, through the resolution of ocean circulation equations (Pedlosky 1996). The work of Maulik et al. is a good example on how complex the parametrization of lateral eddy viscosity can be (Maulik 2016).

Additionally, the boundary conditions at the bottom of the ocean and at sidewalls are still unknown. Numerous numerical boundary conditions can reasonably be applied to ocean models to describe the interaction between the fluid and the ocean boundaries, but none can reflect what happens in the real ocean, largely due to the difficulty in conducting any such observation (Pedlosky 1996). Yet, the choice of

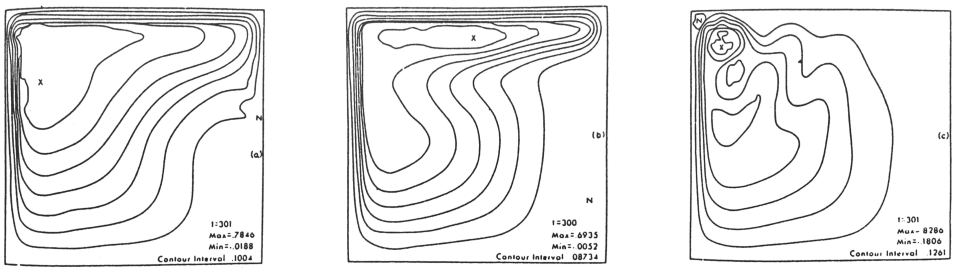

Figure 1.1: Fluid streamlines for different scenarios (a) bottom friction only, (b) lateral friction with slip, and (c) lateral friction with no-slip boundary conditions (Blandford, 1971).

boundary conditions in ocean models impacts much of the fluid circulation, as can be seen in Figure 1.1. The figure shows fluid streamlines for different boundary conditions (Blandford 1971). It is thus consequential to wonder about the extent to which friction and boundary conditions actually affect the ocean circulation.

Based on a strong desire to better understand the role of friction as outlined above, the present work is part of a preliminary study within a broader collective project. Such project has the ambition of testing the validity of existing assumptions about bottom and lateral friction through a series of observations in the Swedish fjord of Gullmarn.

1.2 The Gullmarn Fjord

The Gullmarn fjord is located on the Swedish Skagerrak coast (Figure 1.2). It is approximately 28 km long and 1-3 km wide, with a sill depth of 43 m and a maximum depth of 120 m (Arneborg 2004). The fjord is stratified and the annual mean freshwater input from land into the fjord is 22 $m^3 \cdot s^{-1}$, coming mostly from the river Örekilsälven, located at the fjord extremity (Croot 2003). The Gullmarn fjord makes an ideal location to study estuarine circulation thanks to the the historical Bornö Marine Research Station, situated on Stora Bornö island, about 15 km northeast of Lysekil. One most notable advantage of the station, beside its convenient location, is the hanging bridge from where it is possible to conduct observations down to 33 m of depth, as it has already been done by Arneborg et al. (Arneborg 2001; Arneborg 2004).

Figure 1.2: The Gullmarn Fjord. *Google Maps*, 2019, maps.google.com.

1.3 Presentation of the work

The present Thesis adopts the General Estuarine Transport Model (GETM) to simulate the hydrographic conditions of a simplified version of the Gullmarn Fjord under different scenarios: bottom, vertical, and lateral frictions, each taken independently. To determine how sensitive the idealized fjord circulation is to those processes, the model relies on the alteration of three parameters: the fjord bottom roughness, the Smagorinsky constant, and the vertical eddy viscosity. The different scenarios resulting from those changes are described in Table 3.1.

The present work aspires to enquire whether the idealized version of the Gullmarn fjord is indeed sensitive to friction variations and where the eventual friction changes would be felt the most. Following the present Introduction, the Thesis is articulated into five parts. The first part lays out a basic description of the ocean circulation equations, thus leading to a discussion about the origin and validity of assumptions on friction. Part two puts forth the methodology used for the experiments. Part three offers a description of the outcome of such experiments. Finally, the Thesis ends with a brief conclusive discussion, as a way to pave the path forward. The Thesis is further comprised of an Annex where additional plots are available for review.

2. Friction & ocean circulation

This chapter is divided into two parts. The first one deals with the basic physical equations necessary to grasp the origin and concept of eddy viscosity. The second one briefly introduces the Sverdrup theory to understand the complexity and relevance of friction parametrisation in numerical models.

From a very general perspective, the ocean circulation is driven by the sun, the moon and tectonic movements. While the sun provides heat and water vapor that fuel the thermohaline fluxes as well as surface wind stress, the moon's tides are responsible for internal ocean turbulence and mixing. Earthquakes may create irregular waves, sometimes tsunamis. The above forcings results in complex ocean processes and phenomena, each within a wide range of time and spatial scales, as can be seen in Figure 2.1, thus making it difficult to resolve all of them in numerical models. Small-scale motions are usually parametrized as eddy viscosity, which tunes numerical models and considerably eases the calculations behind them. However, eddy parametrization does not always come from robust physical theory or observation and has a non-negligible impact on the accuracy of numerical ocean models, as shown in Figure 1.1. This chapter describes where friction intervenes in the equations of motion and how it impacts ocean circulation.

2.1 Basic equations of the ocean circulation

In this section, the equations of motion and the equation of continuity will be introduced, and followed by a brief paragraph on the link between friction in ocean circulation and viscosity.

2.1.1 The equations of motion

The equations of motion, or equations of linear momentum conservation, express how the fluid velocity changes for temporal and spatial dimensions (i.e., east, north, and up). They are derived from Newton's First and Second Law of Motion.

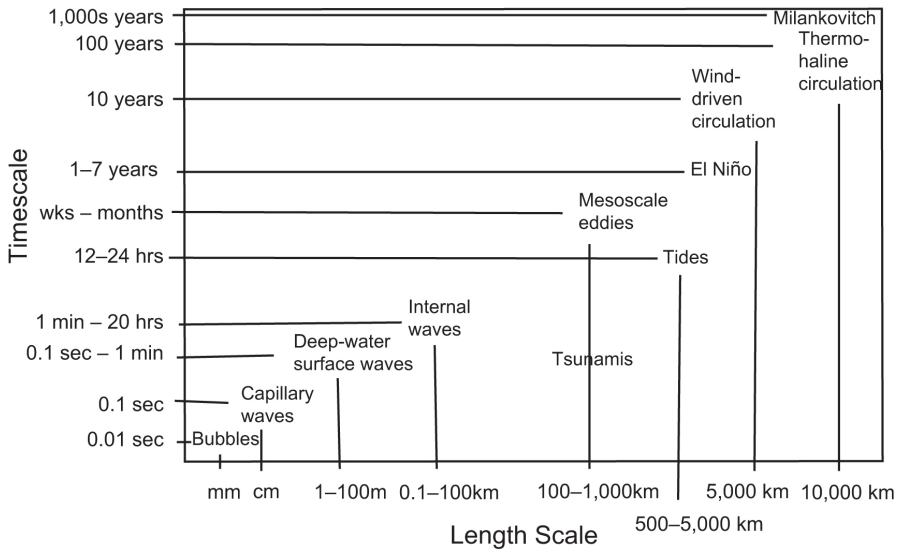

Figure 2.1: Time and space scales of physical oceanographic processes (Talley 2011).

In this thesis, the observation of the fluid parcel is done within an Eulerian framework, at a fixed location relative to the Earth, where $\vec{u} = (u, v, w)$ is the fluid parcel velocity vector in Cartesian coordinates, with u the northward velocity component (x-direction), v the eastward velocity component (y-direction) and w the upward velocity component (z-direction). The unit vectors in northward, eastward, and upward direction are $\hat{x}$, $\hat{y}$ and $\hat{z}$ (respectively).

Therefore, the equation of motion can be written in its vector form as:

$$\underbrace{\frac{D\vec{u}}{Dt}}_{\text{Acceleration}} = \underbrace{-2\vec{\Omega} \times \vec{u}}_{\text{Coriolis acceleration}} - \underbrace{\frac{1}{\rho}\nabla P}_{\text{Pressure gradient force}} + \underbrace{g\hat{z}}_{\text{Gravitational acceleration}} + \underbrace{\frac{\vec{\Im}}{\rho}}_{\text{Friction forces}} \quad (2.1)$$

With:

. $\vec{\Omega}$ the Earth angular velocity

. ϕ the latitude of the fluid parcel, positive in the Northern Hemisphere

. ρ the fluid density

. P the pressure

. g the gravitational acceleration $g = 9.81\ m^2.s^{-1}$

. and $\vec{\Im}$ refers to frictional forces

The total derivative of the fluid parcel velocity $\vec{u}$ can be developed as:

$$\frac{D\vec{u}}{Dt} = \frac{\partial \vec{u}}{\partial t} + (\vec{u} \cdot \nabla)\vec{u} \tag{2.2}$$

The Coriolis acceleration can be expressed as:

$$-2\vec{\Omega} \times \vec{u} = \begin{bmatrix} 2\ \Omega\ sin\phi\ v \\ -2\ \Omega\ sin\phi\ u \\ 0 \end{bmatrix} = \begin{bmatrix} fv \\ -fu \\ 0 \end{bmatrix} \tag{2.3}$$

With f the Coriolis parameter and $f = 2\Omega sin\phi$.

For each coordinate x, y and z, the equations of motion can be expressed as:

$$\text{x-direction :} \qquad \frac{Du}{Dt} = fv - \frac{1}{\rho}\frac{\partial P}{\partial x} + \frac{\Im^x}{\rho} \tag{2.4}$$

$$\text{y-direction :} \qquad \frac{Dv}{Dt} = -fu - \frac{1}{\rho}\frac{\partial P}{\partial y} + \frac{\Im^y}{\rho} \tag{2.5}$$

$$\text{z-direction :} \qquad \frac{Dw}{Dt} = -\frac{1}{\rho}\frac{\partial P}{\partial z} - g + \frac{\Im^z}{\rho} \tag{2.6}$$

Friction in equation 2.1 is generally due to horizontal and vertical stresses (Smagorinsky 1963) and is expressed as a viscous force which renders the oceanic flow smoother. Such friction includes the effect of unresolved small-scale motions such as eddies and is thus often called *eddy viscosity*. However, it is not clear how the eddy viscosity term should be expressed (Pedlosky 1987) and it will be briefly introduced in section 2.1.3. But in this section, the friction term will simply be expressed as the sum of a lateral friction term and a bottom friction term, as:

$$\vec{\Im} \quad = \quad \underbrace{\mu\nabla^2\vec{u}}_{\text{Lateral friction}} \quad - \quad \underbrace{\kappa\vec{u}}_{\text{Bottom friction}} \tag{2.7}$$

With:

. $\mu\nabla^2\vec{u}$ the dissipation originating from lateral friction

. $-\kappa\vec{u}$ the dissipation coming from bottom friction

The friction terms detailed in this paragraph come from an over-simplification of the realistic phenomena. Nonetheless, this simplification not only allows for realistic enough predictions of the ocean circulation, when appropriately tuned (Jochum 2008), but it also facilitates greatly the resolution of the fluid equations (Pedlosky 1996).

2.1.2 The continuity equation

This sections introduces the equation of continuity and the main assumptions behind it. The concepts leading to the equation of continuity of volume are explained in more details in Pond's *Introductory Dynamical Oceanography* (Pond 1983).

The conservation of mass

When modelling the ocean circulation, the conservation of mass, which will be expressed in terms of density in this section, must be fulfilled.

The mass contained in a small volume $\delta x \delta y \delta z$ changes by $\delta x \delta y \delta z \cdot (\frac{\partial \rho}{\partial t})$ per unit of time. The mass conservation can thus be written:

$$\frac{\partial \rho}{\partial t} + \frac{\partial(\rho u)}{\partial x} + \frac{\partial(\rho v)}{\partial y} + \frac{\partial(\rho w)}{\partial z} = 0 \tag{2.8}$$

Additionally, the total derivative of the fluid density can be expressed as:

$$\frac{D\rho}{Dt} = \frac{\partial \rho}{\partial t} + u\frac{\partial(\rho)}{\partial x} + v\frac{\partial(\rho)}{\partial y} + w\frac{\partial(\rho)}{\partial z} = 0 \tag{2.9}$$

And combining 2.8 with 2.9, leads to:

$$\frac{1}{\rho}\frac{D\rho}{Dt} + \frac{\partial(u)}{\partial x} + \frac{\partial(v)}{\partial y} + \frac{\partial(w)}{\partial z} = \frac{1}{\rho}\frac{D\rho}{Dt} + \nabla \cdot \vec{u} = 0 \tag{2.10}$$

The Boussinesq approximation

The Boussinesq approximation is applied when density variation can be neglected, except for the buoyancy term $\rho\vec{g}$. The density ρ can thus be replaced by a constant

density ρ_0, except in the said buoyancy term. With the Boussinesq approximation, the volume changes in the ocean interior are considered small, and the fluid is assumed to be incompressible[1]. With this in mind, the equation of conservation of mass can be simplified as follow:

$$\frac{\partial(u)}{\partial x} + \frac{\partial(v)}{\partial y} + \frac{\partial(w)}{\partial z} = \nabla \cdot \vec{u} = 0 \tag{2.11}$$

2.1.3 Friction in more details

So far, friction has been introduced in the equation of motions, and it was expressed as viscosity. However, the viscosity due to vertical and lateral friction should not be confused with molecular viscosity.

Molecular viscosity is a force driven by the internal motion of fluid molecules with each other. The effect of molecular viscosity can be observed when comparing how honey flows through a straw compared to water: water, with a low molecular viscosity, will flow faster than honey, which has a higher molecular viscosity. When considering large-scale ocean circulation, molecular viscosity is often considered negligible. Indeed, for a Newtonian fluid [2], the relation between molecular viscosity and velocity shear is linear. In this relation, the coefficient of proportionality is the dynamic viscosity η, expressed in $\mathrm{kg} \cdot \mathrm{m}^{-1} \cdot \mathrm{s}^{-1}$. The kinematic viscosity ν can be expressed with the dynamic viscosity η and the fluid density ρ:

$$\nu = \frac{\eta}{\rho} \tag{2.12}$$

Sea water kinematic viscosity is $1.8 \times 10^{-6} \mathrm{m}^2 \cdot \mathrm{s}^{-1}$ at 0°C and $1.05 \times 10^{-6} \mathrm{m}^2 \cdot \mathrm{s}^{-1}$ at 20°C. If we assume that such molecular viscosity does not depend on space, the viscous stress can be expressed in the equation of motion as:

$$\text{x-momentum molecular dissipation} = \nu\left(\frac{\partial^2 u}{\partial x^2} + \frac{\partial^2 u}{\partial y^2} + \frac{\partial^2 u}{\partial z^2}\right) \tag{2.13}$$

And with ν of the order of 10^{-6}, the molecular viscosity can indeed be considered negligible compared to other terms in the momentum equation.

[1] A fluid is incompressible when its volume does not depend on pressure

[2] A Newtonian fluid is defined as a fluid which viscous stress is proportional to the shear stress.

Molecular viscosity can be neglected in the momentum equations because of its small scale of application. However, observations of the ocean circulation show that mixing at larger scales is done by turbulence. Turbulence stirs the water and deforms it into slender filaments. Each smaller scale turbulence deforms the fluid until it reaches a scale small enough to be affected by molecular viscosity. This dissipative process is called *eddy viscosity* and is not to be confused with molecular viscosity.

Similarly to molecular viscosity, eddy viscosity is proportional to turbulent velocities. By definition, the horizontal eddy viscosity refers to turbulent stirring along the x and y directions in Cartesian coordinates, and the vertical eddy viscosity refers to stirring along the z-axis. The coordinate system is sometimes modified as to refer to eddy viscosity along or across isopycnals, but this thesis relies on the original definition.

In the momentum equation 2.4, the viscosity term is thus replaced by the eddy viscosity, and can be expressed in the x-direction as:

$$\text{x-momentum eddy dissipation} = \frac{\partial}{\partial x}(A_H \frac{\partial u}{\partial x}) + \frac{\partial}{\partial y}(A_H \frac{\partial u}{\partial y}) + \frac{\partial}{\partial z}(A_V \frac{\partial u}{\partial z}) \quad (2.14)$$

With

- A_H the spatially dependent horizontal eddy viscosity in $\mathrm{m}^2.\mathrm{s}^{-1}$;
- A_V the spatially dependent vertical eddy viscosity in $\mathrm{m}^2.\mathrm{s}^{-1}$;

The spatial dependence of eddy viscosity makes sense because turbulence is usually distributed heterogeneously in the fluid.

2.2 The Sverdrup theory

This present section briefly introduces the Sverdrup theory to understand the complexity and relevance of friction parametrisation in numerical models.

Pressure maps of the upper ocean, such as Figure 2.2, suggest a clockwise flow in the subtropical North Hemisphere oceans, while a counter-clockwise flow can be observed in the Southern Hemisphere. In each case, the western boundary of the ocean basins are characterised by a swift northward flow, known as the Western

boundary currents. In the North Atlantic, this refers to the Gulf Stream; while in the North Pacific, this corresponds to the Kuroshio current.

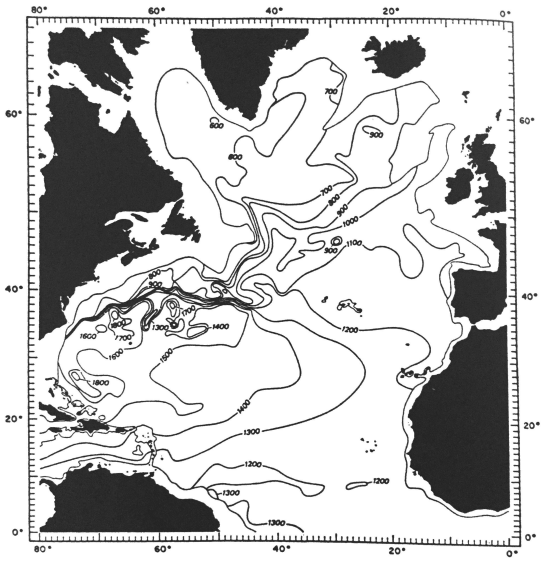

Figure 2.2: Isobars in the North Atlantic subtropical gyre (Stommel 1978). Assuming the North Atlantic flow is in geostrophic balance, the velocity would go along the isobars.

In 1947, Sverdrup published a theory that explains this large-scale subtropical circulation by considering a simplified steady, homogeneous ocean forced by wind stress and without friction (Sverdrup 1947). This section briefly introduces the Sverdrup theory and two of its limitations, based on Pedlosky's *Ocean Circulation Theory* (Pedlosky 1996). This part aims at setting the basis to understand why friction might have a non-negligible impact upon ocean circulation.

2.2.1 A simplified momentum equation for the interior ocean

The momentum equation can be written as detailed in 2.1:

$$\frac{D\vec{u}}{Dt} + 2\vec{\Omega} \times \vec{u} = -\frac{1}{\rho}\nabla P + \vec{g} + \frac{\Im}{\rho} \tag{2.15}$$

With

. Ω the Earth's angular velocity ($7.3\text{x}10^{-5}\text{s}^{-1}$),

. $\vec{u}$ the velocity of the fluid in the rotating referential,

. $\vec{g}$ the acceleration related to gravity and,

. $\Im$ the dissipative effect of small scale turbulence on the large scale circulation momentum.

This form of the momentum equation is still too general to infer any intuitive idea on the dynamical processes behind the ocean circulation. Hence, the next step is based on making a series of approximations focusing on the interior ocean circulation.

Approximation 1: A small Rossby number R_0

For this first approximation, the relative acceleration is compared to the Coriolis acceleration, as expressed in the momentum equation 2.1. Let us consider U a characteristic velocity for the ocean horizontal circulation, and L a characteristic horizontal scale of that same circulation, away from the western boundary. A steady state is commonly assumed for the large-scale ocean circulation, which leads the relative acceleration to be of the following order:

$$\text{relative acceleration} = \frac{D\vec{u}}{Dt} = \mathcal{O}(\frac{UU}{L}) \tag{2.16}$$

and the Coriolis acceleration to be of the order:

$$\text{Coriolis acceleration} = 2.\vec{\Omega} \times \vec{u} = \mathcal{O}(2\Omega sin\theta U) \tag{2.17}$$

The Rossby number, defined as the ratio of the relative acceleration to the Coriolis acceleration, is thus:

$$R_0 \equiv \frac{UU}{2\Omega sin\theta UL} = \frac{U}{fL} \tag{2.18}$$

With

. f the Coriolis parameter defined as $f = 2\Omega sin\theta$ and,

. θ the latitude.

The Sverdrup theory focuses on large scale flows, away from the western boundary, thus typical midlatitudes values for U, L and f can be chosen as follows:

U	L	f
1 $cm.s^{-1}$	1000 km	$10^{-4}s^{-1}$

With those characteristic values, we have:

$$R_0 \equiv 10^{-4} \tag{2.19}$$

By assuming a small Rossby number, the relative acceleration can be neglected before the Coriolis acceleration, making the first approximation for the Sverdrup theory.

Approximation 2: A small horizontal Ekman number E_H

For the second approximation, the frictional force $\Im$ is compared to the Coriolis acceleration. The frictional force due to turbulence $\Im$ is usually expressed as the sum of $\vec{\tau}$ the vertical divergence of horizontal stress on the fluid horizontal surfaces and the horizontal divergence of horizontal stress on the fluid vertical surfaces. The second term is often considered as equivalent to a fluid viscosity caused by smaller scale eddies. The frictional force $\Im$ is thus expressed as:

$$\Im = \frac{\partial \vec{\tau}}{\partial z} + \Im_H \tag{2.20}$$

with

$$\Im_H = \rho A_H \nabla^2 \vec{u} \tag{2.21}$$

and with

. $\vec{\tau}$ the vertical divergence of the horizontal stress,

. z the coordinate in the vertical direction,

. A_H a turbulent viscosity coefficient and,

. ρ the fluid density.

The horizontal Ekman number, defined as the ratio of $\Im_H$ to the Coriolis acceleration, is thus:

$$E_H \equiv \frac{A_H U}{L^2 f U} = \frac{A_H}{f L^2} \tag{2.22}$$

To estimate the horizontal Ekman number E_H for a typical large scale flow in the ocean interior, characteristic values for A_H, f and L are thus considered. It is experimentally challenging to estimate the coefficient A_H, and the literature on eddy-resolving models gives orders ranging from 10^8 $cm^2.s^{-1}$ (Bryan, 1987) to 10^6 $cm^2.s^{-1}$ (Brown and Owens, 1981). It is thus approximated that E_H is smaller than unity and that $\Im_H$ can be neglected before the Coriolis acceleration.

Working with the simplified momentum balance

By neglecting the relative acceleration and $\Im_H$, the momentum equation is thus simplified:

$$\rho f \vec{z} \times \vec{u} = -\nabla P + \frac{\partial \vec{\tau}}{\partial z} \tag{2.23}$$

with $\vec{z}$ the unit vector in the upward vertical direction.

Taking the curl of 2.23 allows for the elimination of the pressure gradient term:

$$\nabla \cdot \rho f \vec{u} = \frac{\partial \vec{z}}{\partial z} \cdot \nabla \times \vec{\tau} \tag{2.24}$$

As the density variations in the ocean interior are of the order of magnitude 10^{-3}, and given that the velocity changes by its own order over the large scale ocean circulation, the fluid density ρ is considered constant and taken out of the divergence in equation 2.24, which gives:

$$\rho \nabla \cdot f \vec{u} = \frac{\partial \vec{z}}{\partial z} \cdot \nabla \times \vec{\tau} \tag{2.25}$$

Introducing the continuity equation

The ocean water is approached as an incompressible fluid. Therefore, the equation of mass conservation can also be written as a volume conservation:

$$\nabla \cdot \vec{u} + \frac{\partial w}{\partial z} = 0 \tag{2.26}$$

By combining the above continuity equation 2.26 with the momentum equation 2.25 comes the following:

$$\rho \beta v = \rho f \frac{\partial w}{\partial z} + \frac{\partial}{\partial z} \vec{z} \cdot \nabla \times \vec{\tau} \tag{2.27}$$

with β the northward spatial derivative of f, i.e.:

$$\beta = \frac{1}{R}\frac{\partial f}{\partial \theta} = \frac{2\Omega cos\theta}{R} \tag{2.28}$$

Considering a two-layer ocean

The Sverdrup theory introduces two layers in the ocean water column:

. The upper mixed layer, of depth h_m, where the vertical flux of horizontal momentum caused by small scale turbulence is non negligible;

. The geostrophic region, below the mixed layer, of depth D, where the above turbulent mixing is considered negligible.

In the geostrophic region, as the turbulent mixing is neglected, the momentum equation can be simplified as it follows:

$$\rho f \vec{z} \times \vec{u} + \nabla P = 0 \tag{2.29}$$

And by using the continuity equation 2.26 for the geostrophic region, below the upper mixed layer, the *Sverdrup relation* can be inferred:

$$\beta v = f\frac{\partial w}{\partial z} \tag{2.30}$$

Physically, the Sverdrup relation states that the vorticity production of a vertically stretched fluid in the water column (i.e. when $\frac{\partial w}{\partial z} > 0$) is proportional to its stretching times the planetary vorticity f. In other words, when the water column is stretched, vorticity increases. In the ocean interior, below the upper mixed layer, the relative vorticity is negligible compared to the planetary vorticity. Therefore, an increase in vorticity must come from the planetary vorticity, which means that the fluid element must move to higher latitudes[3] in order to increase its vorticity.

[3]In the Northern hemisphere, the fluid element would move northwards to increase its vorticity.

2.2.2 A vertical integration of the momentum balance

In the second part of the Sverdrup theory, as detailed in *Ocean Circulation Theory* (Pedlosky 1996), a vertical integration of the momentum balance 2.27 and more approximations lead to the Sverdrup balance relation between the vertically integrated meridional flow and the surface wind stress.

The vertical integration of the simplified momentum equation 2.27 between the top and bottom of the entire water column leads to:

$$\rho_0 \beta \int_{bottom}^{top} v dz = \rho_0 f (w_{top} - w_{bottom}) + \vec{z}.\nabla \times (\vec{\tau}_{top} - \vec{\tau}_{bottom}) \tag{2.31}$$

At this final stage, more approximations become necessary in order to simplify the relation 2.31. It is thus assumed that:

. The time average large scale velocity at the ocean surface is zero, due to the strong gravitational stability of the interface, which brings $w_{top} = 0$;

. The velocity of the fluid at the bottom of the ocean as well as the bottom stress are supposed negligible, which leads to $w_{bottom} \equiv 0$ and $\vec{\tau}_{bottom} \equiv 0$.

These two approximations simplify the equation 2.31:

$$\beta V_S \equiv \frac{1}{\rho} \vec{z}.\nabla \times \vec{\tau}_{top} \tag{2.32}$$

and thus lead to the *Sverdrup balance*:

$$\beta \int_{bottom}^{top} v dz \equiv \frac{1}{\rho} curl(\vec{\tau}) \tag{2.33}$$

With

$$V_S = \int_{bottom}^{top} v dz \tag{2.34}$$

and

$$curl(\vec{\tau}) \equiv \vec{k}.\nabla \times \vec{\tau}_{top} \tag{2.35}$$

Given the principle of continuity at the ocean surface, $\vec{\tau}_{top}$ is often meant as the surface wind stress $\vec{\tau_{wind}}$.

Physically, the Sverdrup balance links the meridional transport of fluid elements in the water column to the surface wind stress, independently from the ocean stratification or the distribution of the wind stress. Indeed the Sverdrup balance does not take into account any vertical structure of the ocean.

2.2.3 Limitations of the Sverdrup theory

One notable limitation of the Sverdrup theory resides in the neglect of the bottom friction. Indeed, to obtain the Sverdrup balance 2.33, the turbulence occurring at the bottom of the ocean has been ignored in two ways:

. The fluid velocity at the bottom of the ocean was neglected, which could be non-zero in case of a sloping ocean bottom;

. The bottom stress itself was then neglected as well.

The bottom stress in the ocean is often studied via its effect, that is, a vertical velocity coming out of the bottom boundary layer. From Ekman layer theory (Ekman 1905), the vertical velocity due to the bottom stress can be expressed as it follows:

$$w_b = \frac{\delta_E}{2}\zeta_b \tag{2.36}$$

with δ_E the bottom boundary layer thickness and ζ_b the fluid vorticity on top of the same boundary layer. Let us now consider the order of w_b:

$$w_b = \mathcal{O}(\frac{\delta_E U}{L}) \tag{2.37}$$

Using the Sverdrup relation in the geostrophic layer as detailed in (Pedlosky 1996), of a constant thickness D, the equation 2.30 leads to:

$$w_b = \mathcal{O}(\frac{\delta_E}{D} \cdot \frac{f}{\beta L})w_E \tag{2.38}$$

with w_E the wind-driven vertical velocity in the mixed layer. It would be sensible to neglect the bottom stress if the ratio $\frac{\delta_E}{D}$ was proven to be bigger than the ratio

$\frac{f}{\beta L}$. In the ocean interior, the first term is about $\frac{1}{6}$ while the second is smaller (Pedlosky 1996).

However, when the geostrophic region thickness D is not constant, as in the case of a sloping ocean bottom, and with $\vec{u_b}$ the horizontal velocity at the very top of the bottom boundary layer, the vertical velocity generated by topography changes is of the order of:

$$w_b = \mathcal{O}(\vec{u_b} \cdot \nabla D) \tag{2.39}$$

If the slope is only of 1 km for 1000 km distance, then a bottom velocity of 0.1 cm.s^{-1} would generate a vertical velocity of about 10^{-4} cm.s^{-1}, which is of an order comparable to the subtropical gyres velocity attributed to the Ekman pumping (Pedlosky 1996). As important bottom velocities can be to evaluate the validity of the Sverdrup balance, it is not sure that the bottom flow even exists given the difficulties to measure it.

Another limitations of the Sverdrup theory lies in neglecting the sidewall friction. In order to obtain the Sverdrup relation 2.30, the sidewall stress was ignored, as the focus was on the circulation of the interior ocean, far from the western boundary. As powerful as the Sverdrup relation can be in describing the interior ocean motion, it does not match the ocean western boundary conditions. Later contributions by Munk effectively describe the frictional western boundary current (Munk 1950). Munk's work assumes the existence of a western boundary layer driven by processes which have been neglected in the above Sverdrup theory. The western boundary layer solution is then joined to the interior ocean by suitable boundary conditions (Pedlosky 1996).

2.3 Summary

In this chapter, it has been shown that friction neglect or parametrization can have a non-negligible effect on the ocean circulation. It is then plausible to wonder about the extent of ocean models sensitivity to changes in friction.

Despite the complexity of the parametrization problem, the hope of improving the validity of numerical ocean models to reach a more comprehensive understanding of the large scale ocean circulation still motivates oceanographers today. This preliminary study proposes to test such sensitivity to friction on a simple cuboid

model, adapted after the Swedish Gullmarn fjord. The next chapter introduces the methodology of the experiments.

3. Methodology

This chapter deals with a description of the experimental design and the different model setups.

The experiment consists in running the General Estuary Transport Model (GETM) on a simplified version of the Gullmarn Fjord for different bottom and lateral friction scenarios. The goal of such experiment is to enquire whether the bottom roughness, the lateral viscosity coefficient or the vertical eddy viscosity, taken independently, have any substantial impact on the fjord mixing.

3.1 The Model

The idea of creating GETM first came in 1997, from the realization that no 3D model was suitable to study the effect of vertical mixing of nutrient in the North Sea. In 2001, GETM was able to render transport phenomena, stratification, momentum fluxes, pressure gradients, and density among other critical metrics (Burchard 2016). More detailed information about the model can be found in GETM Documentation (Burchard 2016). Today, the model is mostly used across the North Sea and the Baltic sea (Stips 2005) but also in the Aegean Sea (Stips 2006).

Notable equations and assumptions behind GETM

As detailed in GETM documentation (Burchard 2016), GETM resolves the momentum equation and the continuity equations in the three dimensions as described in sections 2.1.1 and 2.1.2. The Boussinesq approximation, as seen in section 2.1.2 and the eddy viscosity approximation, as explained in section 2.1.3, are assumed.

At the bottom of the domain, a no-slip condition is applied to the horizontal velocities, giving:

$$u = 0 \quad and \quad v = 0 \tag{3.1}$$

Lateral boundary conditions depend on whether the boundary is considered open or closed. At an open boundary (in this works it refers to the western boundary), the velocity gradient has to disappear. This results in:

$$(\frac{\partial u}{\partial x})_{\text{western boundary}} = 0 \quad and \quad (\frac{\partial v}{\partial x})_{\text{western boundary}} = 0 \tag{3.2}$$

The northern, southern and eastern boundaries are closed. There, the flow must be parallel to the respective boundary, which gives:

$$u_{\text{eastern boundary}} = 0, \quad v_{\text{northern boundary}} = 0 \quad and \quad v_{\text{southern boundary}} = 0 \tag{3.3}$$

GETM and GOTM

In this experiment, the three-dimensional transport model GETM is coupled to the one-dimension General Ocean Turbulence Model (GOTM), which is in charge of computing the vertical turbulent mixing in the water column. GOTM uses the main thermodynamic and hydrodynamics processes linked to natural water turbulence modelling[4].

3.2 Setting up the model

3.2.1 The idealized fjord

In all the following experimental setups, a simple cuboid basin is used to represent the Gullmarn fjord, as shows Figure 3.1. The simplified fjord is 28 km long and 500 m wide. Its depth varies from 80 m at the western open boundary to 5 m at the eastern boundary.

The Gullmarn fjord is actually 1-2 km wide (Arneborg 2004). The 500 m width of the idealized fjord has been chosen in regards to the future observation campaign taking place from Bornö Marine Research Station, where the Gullmarn fjord is approximately 500 m wide. With such narrowness, it is sensible to assume that the influence of Coriolis acceleration on the fjord is negligible.

[4]More information about GOTM is available on the online documentation (Umlauf 2012)

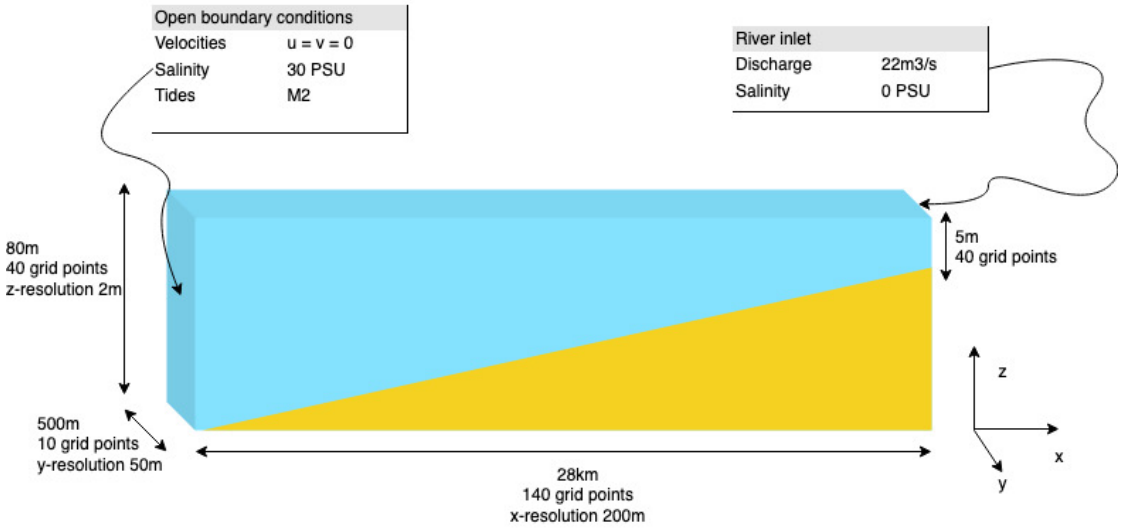

Figure 3.1: Dimensions of the simple cuboid model

3.2.2 Model time-step

The following constraint is applied to the time-step t in order to resolve waves in the fjord:

$$t < \frac{D}{v} \tag{3.4}$$

With

. t the time-step in s,

. D the grid cell dimension in m and,

. v the wave speed in $m.S^{-1}$.

The shallow water theory, described in Pedlosky's *Geophysical Fluid Dynamics* (Pedlosky 1987), and applied to small amplitude motions, gives the shallow-water wave[5] speed:

$$v = \sqrt{gH} \tag{3.5}$$

[5]Whose wavelength is bigger than basin depth.

With

. v the approximated wave speed in $m.S^{-1}$,

. g the gravitational acceleration and $g = 9.81\ m^2.S^{-1}$,

. and H the depth of the basin in meters, here $H = H_{max} = 80m$.

Thus t must abide:

$$t < \frac{D}{\sqrt{gH}} \tag{3.6}$$

and

$$t < \frac{200}{(\sqrt{9.8 \times 80})} = 2.3s \tag{3.7}$$

To comply with this constraint, the model time-step has been fixed at 1 second.

3.2.3 Forcings and initial conditions

Freshwater input

Most of the Gullmarn fresh water inflow comes from storm water runoff and from the river Örekil, whose mean discharge, between the years 1909 and 1990, is about 22 $m^3 \cdot s^{-1}$ (Filipsson 2004). Based on this average, the river discharge coming from the eastern boundary of the simplified fjord as been set to 22 $m^3 \cdot s^{-1}$ in all scenarios of the experiment.

Salinity

The Gullmarn fjord waters are stratified due to difference in salinity and thus density. The topmost layer (up to 15 m deep) contains the least dense waters with a salinity between 24 and 27 PSU. In the intermediate layer (15-50 m approximately), the salinity ranges from 32 to 33. And in the deepest layer, little seasonal variation is observed and the salinity range from 34 to 35 PSU (Filipsson 2004). In the context of this experiment, an initial uniform salinity of 30 PSU has been set.

Tides

The idealized fjord western boundary is open, as can be seen in Figure 3.1. From there, a M2 tide is imposed, whose amplitude is shown in Figure 3.2. It follows

that the only two forcings in the idealized fjord are led by tidal elevation changes and density gradients due to the river inlet.

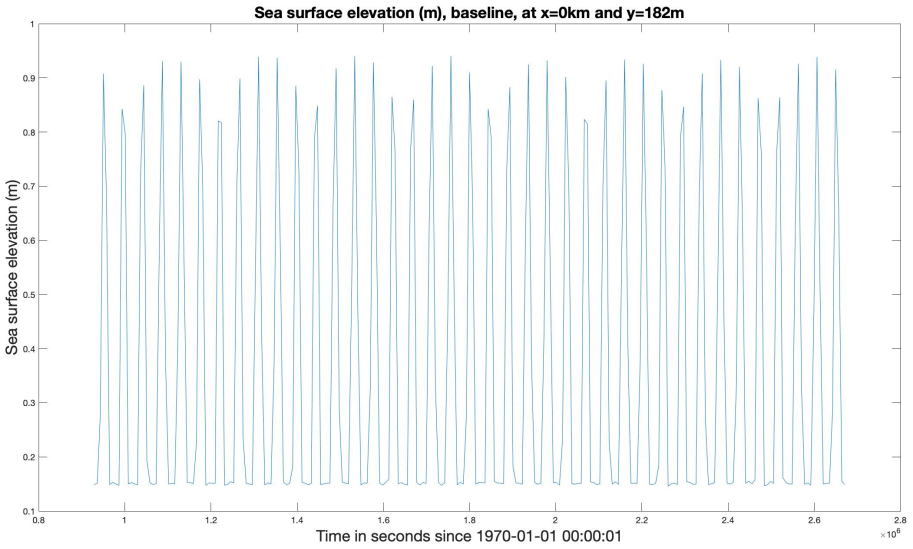

Figure 3.2: Sea surface elevation at the open boundary of the idealized fjord.

At the open boundary, lateral velocities are zero: $u = v = 0$.

What has been ignored in the experiments

In this experiment, the focus being mostly on salinity distribution, temperatures in the fjord are not resolved. Additionally, as the temperature distribution is beyond the scope of this preliminary work, neither meteorological forcing is involved, nor surface wind stress.

3.3 Variations in friction

To determine the fjord sensitivity to frictional forces, three parameters are altered independently: the bottom roughness, the Smagorinsky constant, and the vertical viscosity. The three sections below justify the choice of the said parameters in this experiment.

3.3.1 On the bottom roughness

While laying out the momentum equations, the bottom friction term was expressed in equation 2.7 as $-\kappa\vec{u}$. Considering a no-slip condition and a logarithmic law of

the wall (Burchard 2016; Perlin 2005), the velocity right above the ocean bottom can be expressed as:

$$(u_x^*)^z = \frac{\tau_b^x}{\rho_0} = C_D u^2 \tag{3.8}$$

With

. $(u_x^*)^z$ the flow velocity immediately above the bottom;

. τ_b^x the bottom stress;

. ρ_0 the approximated constant fluid density;

. and C_D the non-dimensional bottom drag coefficient, defined as:

$$C_D = \sqrt{\frac{\kappa}{\ln \frac{z+H+z_0}{z_0}}} \tag{3.9}$$

With

. z_0 the bottom stress;

. z the grid-cell distance from the wall ;

. and H the water depth.

It is worth noting that the bottom roughness z_0 depends on a constant bottom roughness $z_0^{constant}$ and the bottom velocity. GETM works with GOTM through iterations to obtain realistic values of bottom roughness and bottom velocity.

A change in bottom roughness z_0 will thus change the drag coefficient C_D and eventually affect the bottom friction term. This is why the bottom roughness has been chosen to simulate a change in bottom friction. Additionally, this parameter is also readily modifiable from GETM input file.

The baseline bottom roughness value from GETM is set at 1.5mm and has not been modified for the control run of this experiment. In the setups 14 and 15 the bottom roughness has been multiplied by 5 and 0.5 (respectively). These bottom roughness values changes seem sensible based on Guillou's study (Guillou 2013).

3.3.2 On the vertical eddy viscosity

GETM is coupled to the one-dimension GOTM. GOTM inputs in GETM components of the vertical turbulent mixing in the water column. This can then be modified by altering the vertical viscosity directly from GOTM[6]. Eddy vertical viscosity from GOTM is thus another parameter that has been selected to simulate changes in friction.

3.3.3 On the Smagorinsky constant

In the previous section, it was mentioned that GETM calls GOTM for vertical viscosity. However, for horizontal viscosity, GETM uses a Smagorinsky-like eddy viscosity parametrisation, which expresses turbulence with a viscosity coefficient that depends on the fluid deformation (Smagorinsky 1963; Burchard 2016).

While laying out the momentum equations, the horizontal friction term was expressed in equation 2.7 as $\mu\nabla^2\vec{u}$. Assuming an isotropic viscosity in the idealized fjord as in Munk's paper (Munk 1950), the horizontal friction can be expressed as introduced by Jochum et al. (Jochum 2008):

$$F_x \;=\; A\,(\partial_x^2 u \;+\; \partial_y^2 u) \tag{3.10}$$

and

$$F_y \;=\; A\,(\partial_x^2 v \;+\; \partial_y^2 v) \tag{3.11}$$

with A the viscosity coefficient, also referred to as the Smagorinsky constant.

Therefore, changing the viscosity coefficient directly from GETM input file allows variations in horizontal eddy viscosity.

It is worth mentioning that, in GETM, the free-slip condition is applied on the sidewall boundaries of the water basin. Hence, the sidewall friction is not taken into account.

Nevertheless, by changing the viscosity coefficient, alteration of the horizontal eddy viscosity is possible.

[6]More information is available in the online GOTM documentation (Umlauf 2012)

Table 3.1 deals with a description of the different experimental scenarios applied to the idealized fjord domain. Setup no. 13 will be referred as control run in the rest of this thesis.

Experimental scenarios			
Setup number	Bottom roughness factor	Vertical viscosity factor	Lateral viscosity coefficient factor
13	1	1	1
14	5	1	1
15	0.5	1	1
18	1	2	1
19	1	5	1
16	1	1	2
17	1	1	$\frac{1}{3}$

Table 3.1: Description of the control run and the six experimental setups. Each parameter is modified independently of the others.

3.4 Summary

This chapter described on one hand the idealized fjord dimensions, forcings and initial conditions; and on the other hand, the experimental design and the three parameters used to vary friction: the bottom roughness, the Smagorinsky constant and the vertical viscosity.

The next chapter first presents the fjord circulation for the control run and then documents the fjord sensitivity to friction.

4. Result analysis

This chapter is divided into two parts. The first part aims at understanding better the idealized fjord circulation for the baseline setup. The second part documents the changes caused by variation in friction through independent modification of the fjord bottom roughness, the Smagorinsky constant, and the vertical viscosity.

4.1 Control run flow in the idealized fjord

4.1.1 Spin-up

To evaluate the spin-up time of the model, the salinity time series was plotted for three locations in the fjords, just below the surface, as seen in Figure 4.1. The points only differ in their distance from the river inlet and they correspond to snapshots, taken every two hours. Steady state is reached at 1×10^6 seconds, which is about 12 days. Consequently, the baseline as well as each of the six experiments were then run for one month.

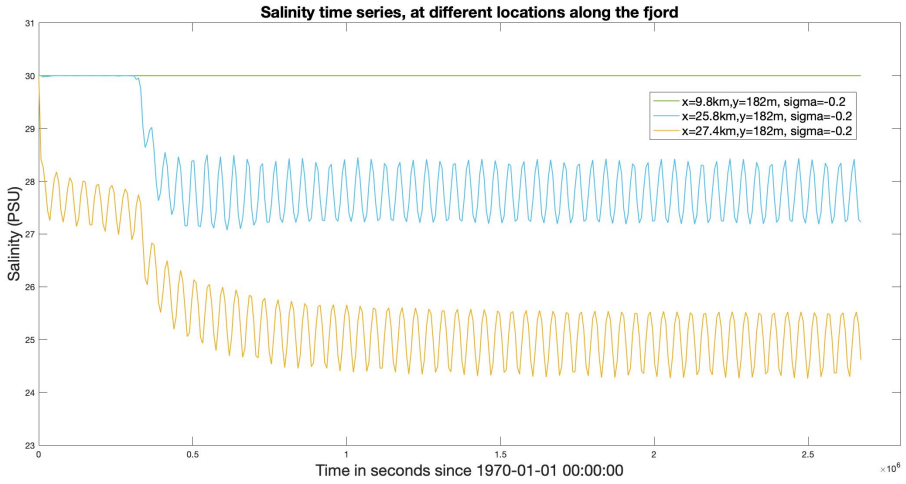

Figure 4.1: Salinity time series for three points along the fjord, near sea surface, and for the baseline setup. In green: x=9.8km, near the open boundary. In blue: x=25.8km. And in yellow: x=27.4km, near the river inlet.

4.1.2 Wave propagation

In order to have an idea about wave propagation in the idealized fjord, the surface elevation has been plotted for the first six time-steps of the baseline model run, as seen in Figure 4.2. Each point correspond to a snapshot, taken every 10 minutes. There seems to be water accumulation on the eastern boundary, which can be explained by the sloping bottom of the idealized fjord at its mouth: the water depth being shallower, the wave speed $\sqrt{gH}$ is reduced, which causes a "traffic-jam" effect, as the water accumulates in this location.

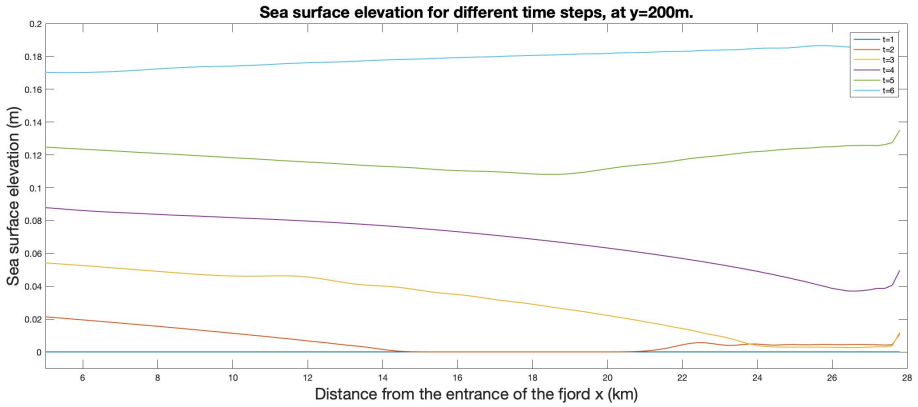

Figure 4.2: Sea surface elevation time series for the first six time steps, baseline run.

4.1.3 Idealized fjord dynamics

To better apprehend the fjord circulation prior to frictions variations, the salinity distribution (Figure 4.3) and the x-direction velocity (Figure 4.4) have been plotted. A typical fjord circulation can be observed: a thinner surface layer flows westwards, and a thicker bottom layer of sluggish water flows eastwards (Farmer 1983).

For the remaining part of the present thesis, sigma levels will be be used instead of the effective depth with the aim of increasing plot visibility. Additionally, each plot shown in the next sections corresponds to the last screenshot taken after one month of model run. Finally, anomalies were calculated by subtracting results from friction variations to the control run.

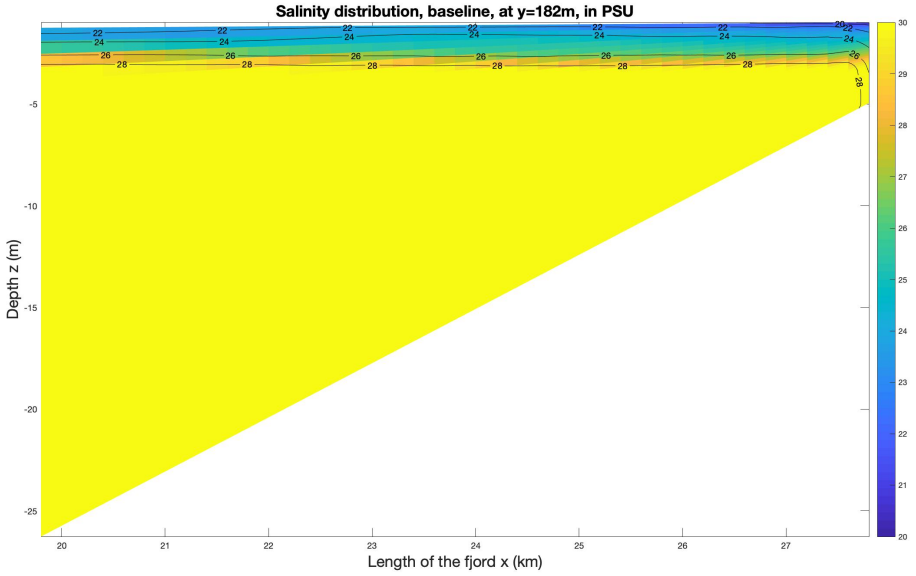

Figure 4.3: Salinity distribution (PSU) in the idealized fjord, baseline, at y=182m, zoomed in at the eastern boundary. The section of the entire fjord is available in the appendix.

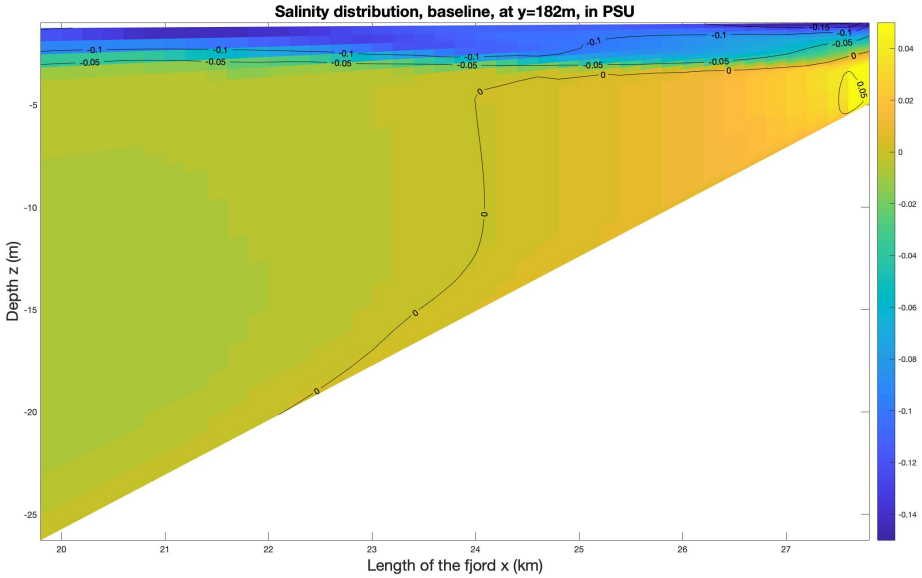

Figure 4.4: x-direction velocity (m/s) in the idealized fjord, baseline, at y=182m, zoomed in at the eastern boundary. The section of the entire fjord is available in the appendix.

4.2 Sensitivity to friction changes: Which parameter matters most?

This project aims at identifying whether friction has a substantial impact upon the idealized fjord circulation. Three parameters have been separately increased: the bottom friction, the lateral viscosity coefficient (affecting the horizontal eddy viscosity), and the vertical eddy viscosity (from GOTM).

With this goal in mind, the salinity distribution anomalies for each parameter increase were plotted, as seen on Figure 4.5. The same has been done with the x-direction velocity, as seen on Figure 4.6. Additionally, the salinity and velocity anomalies for a decrease in bottom friction and lateral viscosity coefficient are given in the Appendix 6.

In Figure 4.5 and Figure 4.6, it can be seen how an increase in the lateral viscosity coefficient, as described in section 3.3.3, substantially affects the salinity distribution and the x-direction velocity; at the same time bottom friction and vertical viscosity have a more discreet impact on both variable studied. Indeed, it can be observed that an increased lateral viscosity coefficient by a factor of 2 allows changes in salinity of up to 1 PSU, especially at the eastern boundary, where the river inlet is located. The x-direction velocity is also affected most at the eastern boundary. Additionally, the same result can be observed in the case of decreased bottom friction and lateral viscosity coefficient: the latter has a more significant impact on the fjord circulation, especially at the eastern boundary. In a study conducted by Glorioso and Davies (Glorioso 1995), it was concluded that the circulation and flushing time of a deep channel estuary would be determined by horizontal processes and it would thus not be very sensitive to changes in vertical eddy viscosity, which is coherent with the present results.

To this point, it has been shown that a doubling of the lateral viscosity coefficient matters significantly in the circulation of the idealized fjord. The next step consists in documenting those changes. Figures 4.7-4.9 correspond to the sensitivity of the salinity distribution, the x-direction velocity, and the standard deviation of the same velocity (respectively) to an increase in the lateral viscosity coefficient by a factor of 2.

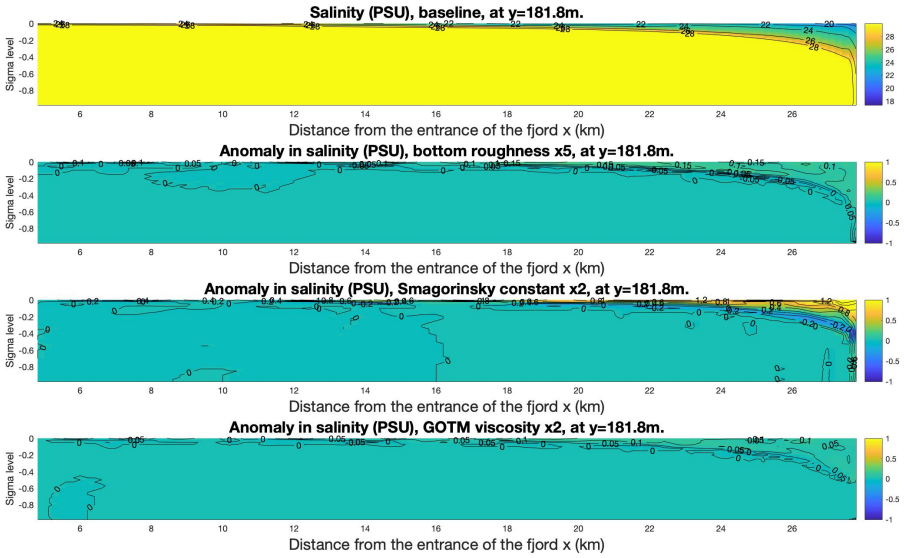

Figure 4.5: Salinity distribution sensitivity to variations in friction. The uppermost plot represents the baseline salinity distribution in the fjord. The lower three plots represent the anomaly in salinity distribution for an increase in bottom friction, lateral viscosity coefficient and vertical viscosity (respectively).

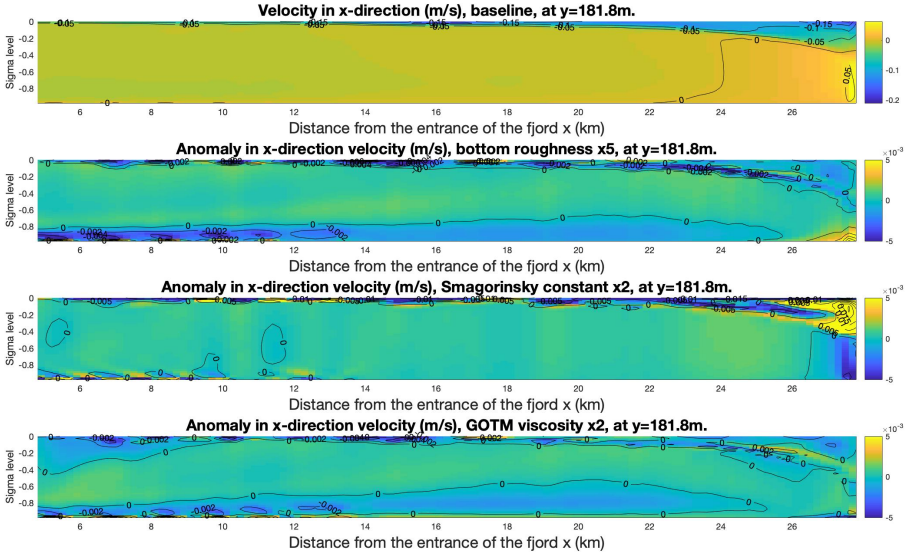

Figure 4.6: x-direction velocity sensitivity to variations in friction. The uppermost plot represents the baseline x-direction velocity in the fjord. The lower three plots represent the anomaly in x-direction velocity for an increase in bottom friction, lateral viscosity coefficient and vertical viscosity (respectively).

All of the four analyzed ocean metrics respond most to a change in lateral viscosity at the eastern boundary. It is then consequential to ask what could cause such changes. Given that only two forcings are part of the idealized model of the fjord circulation, only tides or freshwater pulses could explain why the anomalies are observed in this area.

To enquire about the change at the eastern boundary, the horizontal eddy viscosity was plotted, as seen in Figure 4.10 and Figure 4.11. As the interest is now mainly on the eastern boundary, the Figure 4.12 presents a focused view on the horizontal eddy viscosity in this location. Figure 4.10 suggests that an increase in the Smagorinsky constant also increases the horizontal friction at the sidewall, especially at the eastern boundary of the present idealized fjord.

In both Figure 4.10 and Figure 4.12, an indigo plume can be seen stretching away from the eastern boundary to the middle of the fjord. This horizontal viscosity pattern (Figure 4.13), observed for an increase in the lateral friction, was compared successively to the patterns of salinity distribution (Figure 4.14) and x-direction velocity (Figure 4.15) according to four different sigma levels (thus varying depth due to the sloping bottom). This comparison should identify a likely forcing between density fluctuation and tides that could explain such a pattern. Given that the tides have been shown to matter less than the density fluctuations due to the river discharge, as per the control run flow described in 4.1 and observation in the real Gullmarn fjord (Arneborg 2001), it is also expected to see greater similarity between the horizontal viscosity pattern and the salinity distribution than with the x-direction velocities.

Figure 4.13-4.15 indeed show that the horizontal viscosity pattern corresponds more to the salinity distribution than to the tidal forcing. It is therefore likely that the freshwater pulses in the idealized fjord are more important for the exchange of water properties than the tidal forcing.

To confirm this hypothesis, the baseline experimental setup was run with and without tides. The salinity distribution, x-direction velocity and horizontal viscosity were then plotted for both tidal scenarios. The resulting figures can be found in the Appendix 6. Those results agree with the fact that the tides seem to have a small impact on the idealized fjord circulation at the eastern boundary.

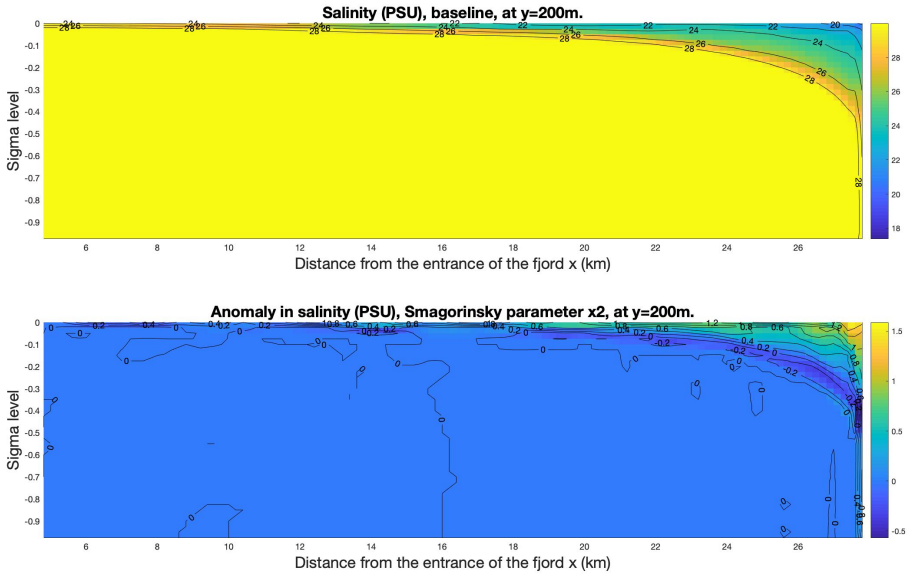

Figure 4.7: Salinity distribution sensitivity to an increase in the lateral viscosity coefficient. The uppermost plot represents the baseline salinity in the fjord. The lower plot represents the anomaly in salinity distribution after the increase in lateral viscosity.

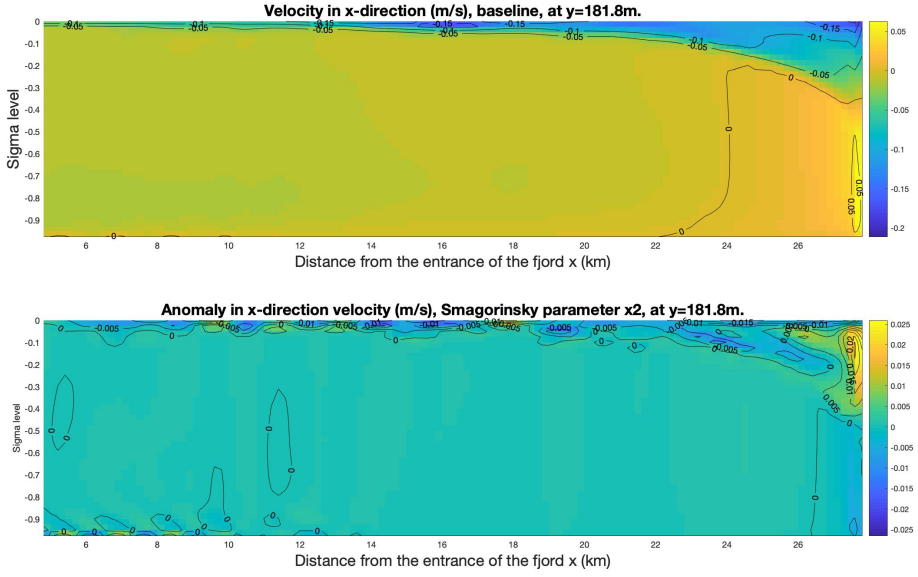

Figure 4.8: x-direction velocity sensitivity to an increase in the lateral viscosity coefficient. The uppermost plot represents the baseline x-direction velocity in the fjord. The lower plot represents the anomaly in the same variable after the increase in lateral viscosity.

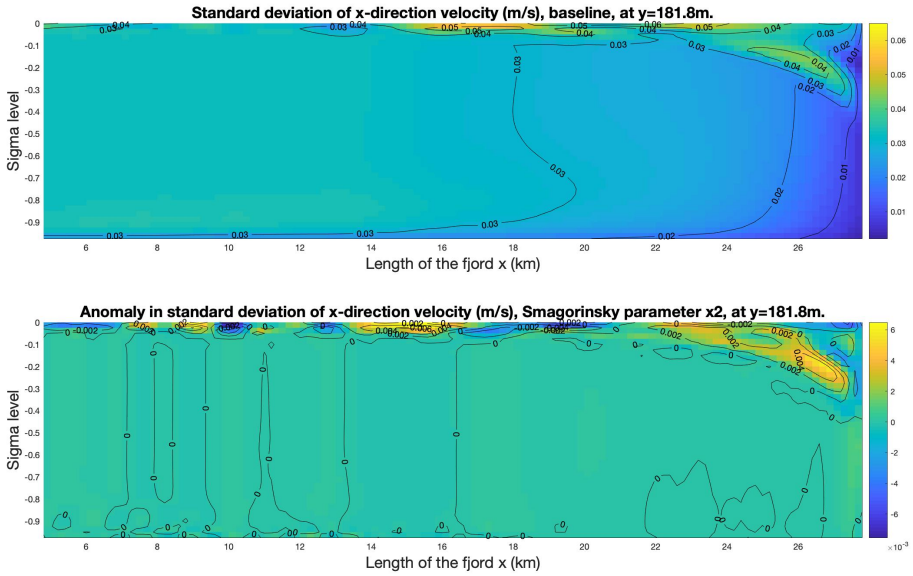

Figure 4.9: Sensitivity of the x-direction velocity standard deviation to an increase in the lateral viscosity coefficient. The uppermost plot represents the baseline x-direction velocity standard deviation in the fjord. The lower plot represents the anomaly in the same variable after the increase in lateral viscosity.

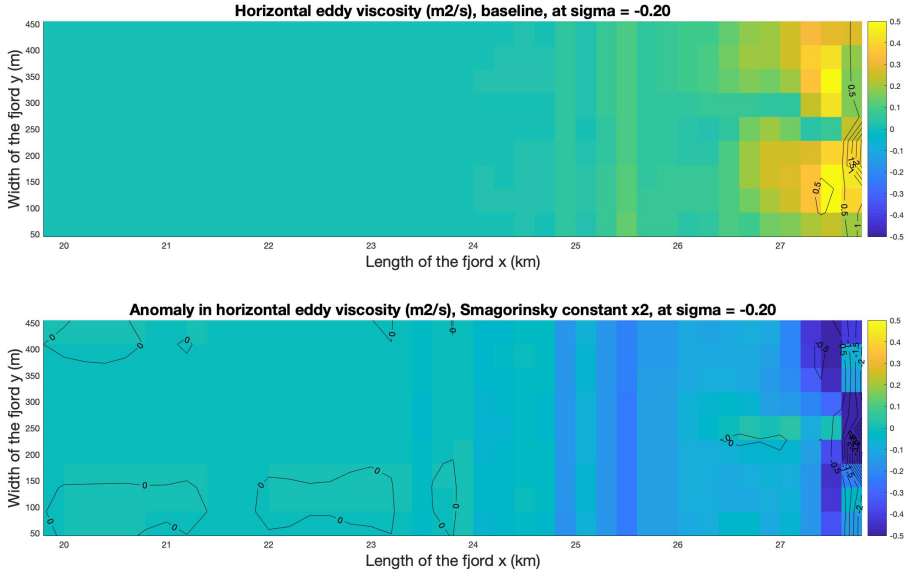

Figure 4.10: Sensitivity of the horizontal eddy viscosity to an increase in the lateral viscosity coefficient. The uppermost plot represents the baseline horizontal viscosity in the fjord, near the surface. The lower plot represents the anomaly in the same variable after the increase in lateral viscosity.

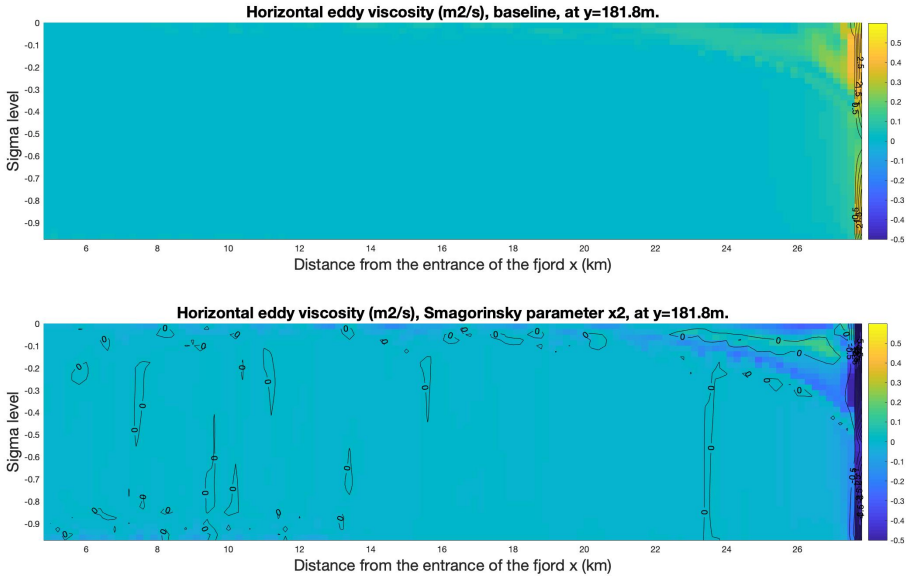

Figure 4.11: Sensitivity of the horizontal eddy viscosity to an increase in the lateral viscosity coefficient. The uppermost plot represents the baseline horizontal viscosity in the fjord. The lower plot represents the anomaly in the same variable after the increase in lateral viscosity.

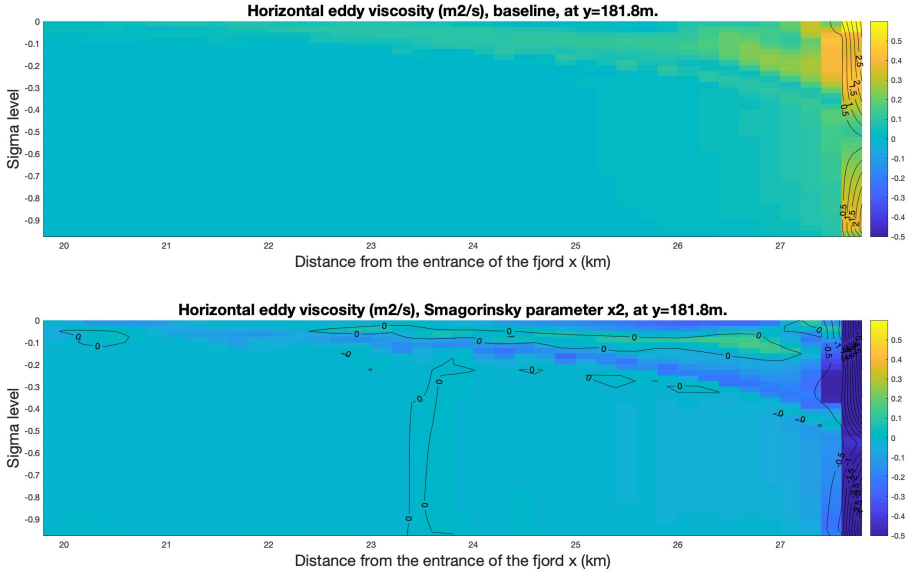

Figure 4.12: Sensitivity of the horizontal eddy viscosity to an increase in the lateral viscosity coefficient, zooming in at the eastern boundary. The uppermost plot represents the baseline horizontal viscosity in the fjord. The lower plot represents the anomaly in the same variable after the increase in lateral viscosity.

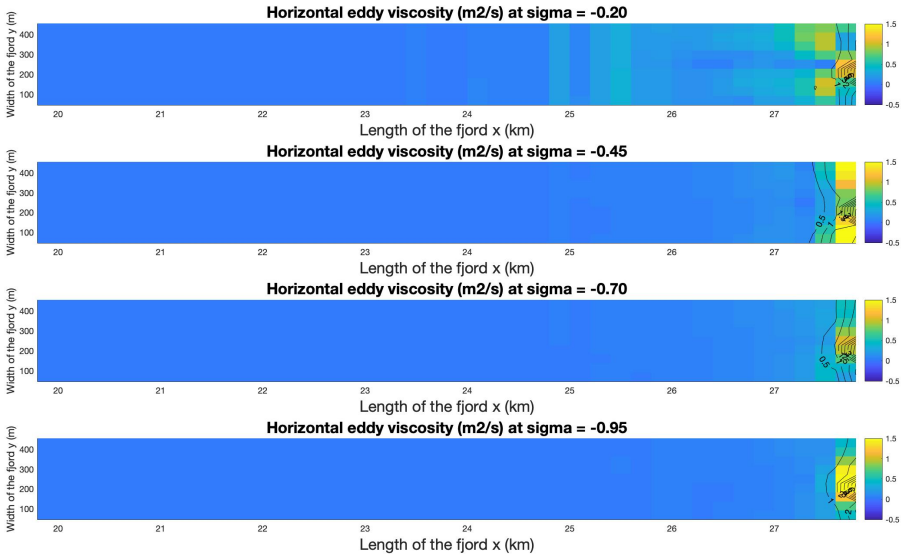

Figure 4.13: Horizontal eddy viscosity for an increase in the lateral viscosity coefficient, zooming in at the eastern boundary. The uppermost plot represents the water just below the surface. The lower plots correspond to increasing depth, along sigma level.

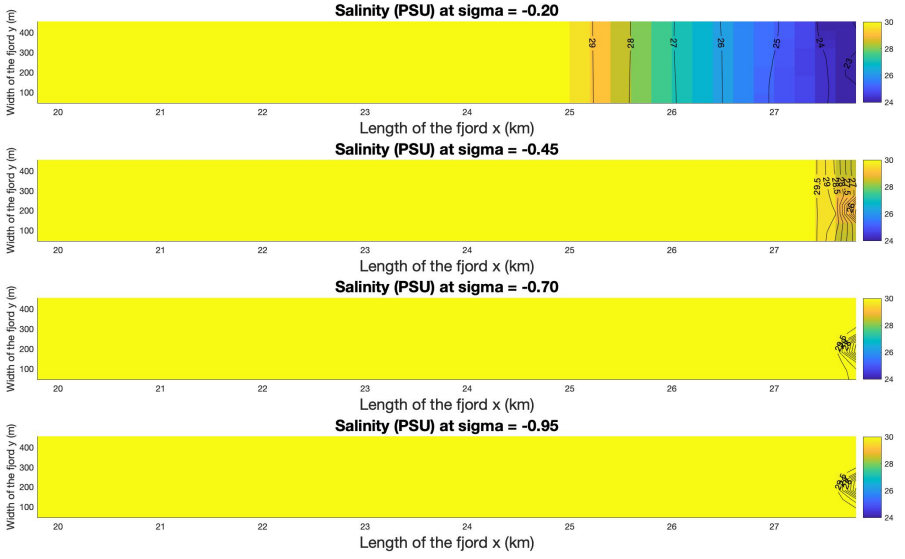

Figure 4.14: Salinity distribution for an increase in the lateral viscosity coefficient, zooming in at the eastern boundary. The uppermost plot represents the water just below the surface. The lower plots correspond to increasing depth, along sigma level.

4.3 Summary

This chapter dealt with a short enquiry about the baseline fjord circulation, before any modification in friction. The second part of the chapter focused on the fjord sensitivity to changes in friction through the variations in its bottom roughness, the Smagorinsky constant and the vertical viscosity. An increase in lateral viscosity, through the Smagorinsky constant, substantially affects the salinity and x-direction velocity distribution in the idealized fjord, especially at the eastern boundary. Bottom friction and vertical viscosity have a more discreet impact on both variables studied. Finally the present idealized fjord seems to be more influenced by density fluctuations than by tidal forcing.

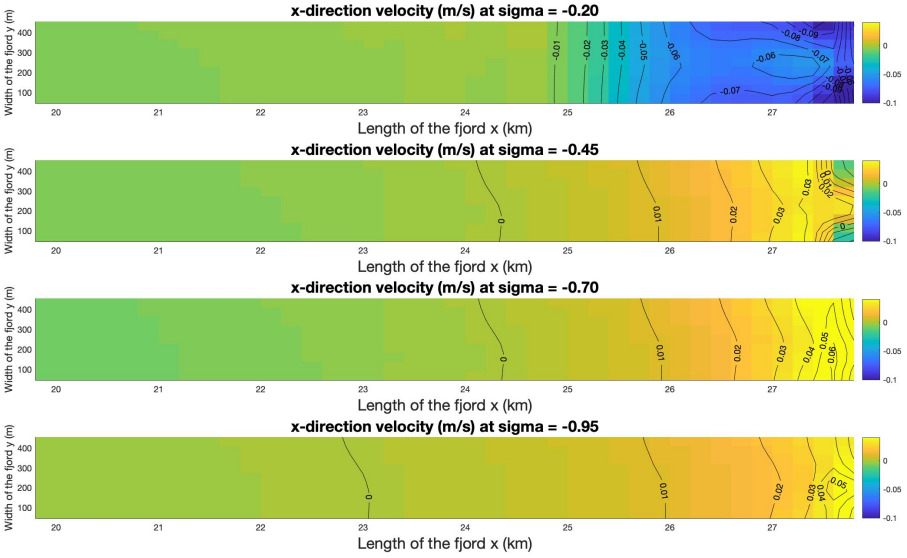

Figure 4.15: x-direction velocity for an increase in the lateral viscosity coefficient, zooming in at the eastern boundary. The uppermost plot represents the water just below the surface. The lower plots correspond to increasing depth, along sigma level.

5. Discussion and conclusion

The goal of this preliminary study was to enquire ocean circulation sensitivity to friction, by using an idealized fjord model. The objective of this present work was to show that, if the estuary responds modestly to independent changes in bottom friction and vertical eddy viscosity, changes due to variations in horizontal eddy viscosity cannot be ignored, especially at the eastern boundary of the fjord. Modelled patterns of horizontal eddy viscosity were compared to salinity and x-direction velocity patterns and showed stronger similarities with density fluctuations than with the tidal flow.

The oversimplification of the fjord geometry and bathymetry described in Figure 3.1 allows for a sensible model run time. It takes less than an hour to perform a one-month model run with the High Performance Computing resources provided by the Danish Center for Climate Computing, which is enough time to reach a steady state, as shown in Figure 4.1. The chosen grid size of 200 m $\times$ 50 m $\times$ 5 m allows sufficient resolution of processes of interest in the fjord, such as density gradient and tidal forcing. However, this specific model would not be suitable for the study of turbulent processes with a spacial scale smaller than 200 m.

Glorioso et al. have shown that the direction of the wind stress (along or cross estuary) significantly impacts the circulation and flushing time of the studied channel (Glorioso 1995). This idea was supported by other works, such as the simple fjord model designed by Klinck et al. (Klinck 1982) and observations by Valle et al. (Valle-Levinson 2014). Accordingly, including wind stress to analyze whether a variation in surface stress would influence the fjord stratification and its sensitivity to friction could be a promising path for further research. Even more so since observations by Arneborg et al. in the Gullmarn fjord suggest that, together with the freshwater discharge from the Örekilsälven, the wind stress plays an important role in the Gullmarn fjord dynamics (Arneborg 2001).

This work is a preliminary study of the Gullmarn fjord in preparation for an observational expedition aiming at studying the fjord circulation and its frictional

components. Thus, this work could also be extended towards a more realistic model of the Gullmarn fjord which would provide more detailed insight to assist the observation project preparation and execution.

Bibliography

1. Arneborg, L. (2001). 'The Internal Seiches in Gullmar Fjord. Part I: Dynamics'. In: *Journal of Physical Oceanography* 31.

2. — (2004). 'Spatial Variability of Diapycnal Mixing and Turbulent Dissipation Rates in a Stagnant Fjord Basin'. In: *Journal of Physical Oceanography* 34.

3. Blandford, R. (1971). 'Boundary conditions in homogeneous ocean models'. In: *Deep Sea Research and Oceanographic Abstracts 18.7, pp. 739 –751.*

4. Burchard, H. (2016). *General Estuarine Transport Model Documentation.* URL: https://getm.eu/.

5. Croot, P. (2003). 'Seasonal cycle of copper speciation in Gullmar Fjord, Sweden'. In: *Limnology and Oceanography* 48.

6. Ekman, V. W. (1905). 'On the influence of the earth's rotation on ocean currents'. In: *Arkiv f. Matem., Astr. o. Fysik (Stockholm) Bd. 2, No. 11, 53pp.*

7. Farmer, D. (1983). 'The Physical Oceanography of Fjords'. In: *Pros. Oceanog. Vol. 12, pp. 147-220,*

8. Filipsson, H. (2004). 'Climate variations, an overlooked factor influencing the recent marine environment. An example from Gullmar Fjord, Sweden, illustrated by benthic foraminifera and hydrographic data'. In: *Estuaries.*

9. Glorioso, P. (1995). 'The influence of eddy viscosity formulation, bottom topography, and wind-wave effects upon the circulation of a shallow bay'. In: *American Meteorological Society.*

10. Goosse, H. (2015). *Climate system dynamics and modelling.* Cambridge University Press.

11. Guillou, N. (2013). 'Modelling impact of bottom roughness on sea surface temperature in the Sea of Iroise'. In: *Continental Shelf Research 54 (2013) 80–92*.

12. Hibiya, T. (2017). 'The impacts of ocean bottom roughness and tidal flow amplitude on abyssal mixing'. In: *J. Geophys. Res. Oceans*.

13. Jochum, M. (2008). 'Ocean viscosity and climate'. In: *J. Geophys. Res.* 113.

14. Klinck, J. (1982). 'A simple model of fjord and coastal circulation interaction'. In: *Journal of Physical Oceanography*.

15. Maulik, R. (2016). 'Dynamic modeling of the horizontal eddy viscosity coefficient for quasigeostrophic'. In: *Journal of Ocean Engineering and Science*.

16. Munk, W. (1950). 'On the wind-driven circulation'. In: *J. Meterol. 7, 79–93*.

17. Pedlosky, J. (1987). *Geophysical Fluid Dynamics*. Springer.

18. — (1996). *Ocean Circulation Theory*. Springer.

19. Perlin, A. (2005). 'A modified law-of-the-wall applied to oceanic bottom boundary layers'. In: *J. Geophys. Res., 110, C10S10*.

20. Pond, S. (1983). *Introductory Dynamical Oceanography*. Springer.

21. Smagorinsky, J. (1963). 'General circulation experiments with the primitive equations - I. The basic experiment'. In: *Monthly Weather Review*.

22. Stips, A. (2005). 'Realistic multiannual simulations of the coupled North Sea and Baltic Sea system using the GETM model'. In: *European Commission, Joint Research Center*.

23. — (2006). 'General Estuarine Transport Model (GETM) Validation by Using In-situ Measurements and Remote Sensing Data in the Aegean Sea'. In: *European Commission, Joint Research Center*.

24. Stommel, H. (1978). 'Dynamic topography and recirculation of the North Atlantic'. In: *J. Mar. Res., 36, 449-468*.

25. Sverdrup, H. U. (1947). 'Wind-driven currents in a baroclinic ocean; with application to the equatorial currents of the eastern Pacific'. In: *Proc. Natl. Acad. Sci. Sci. 33, 318-326.*

26. Talley, L. (2011). *Descriptive Physical Oceanography.* Elsevier Ltd.

27. Umlauf, L. (2012). *GOTM - Sourcecode and Test Case Documentation.* URL: https://gotm.net/.

28. Valle-Levinson, A. (2014). 'Variations of tidally driven three-layer residual circulation in fjords'. In: *O. Ocean Dynamics (2014) 64: 459.*

6. Appendix

6.1 Salinity and velocity distribution in the fjord

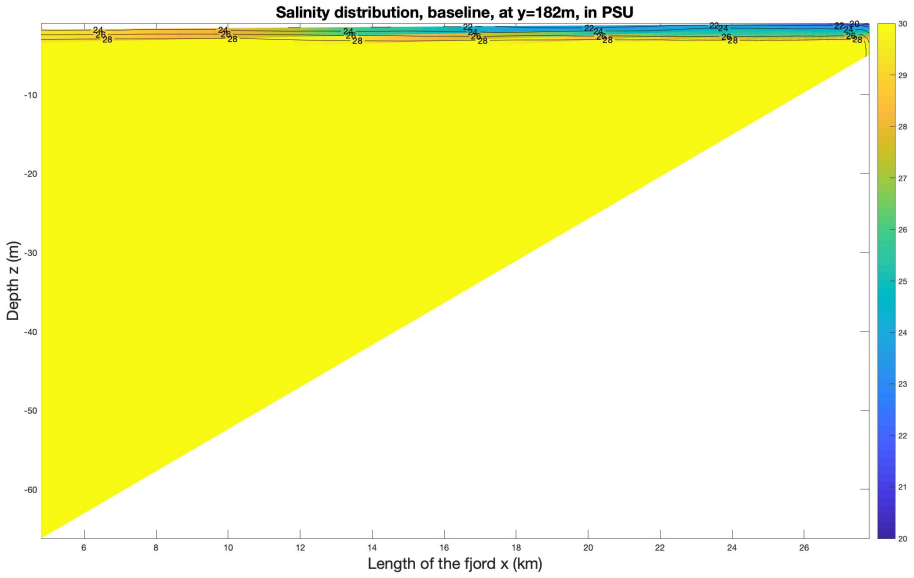

Figure 6.1: Salinity distribution (PSU) in the idealized fjord, baseline, at y=182m.

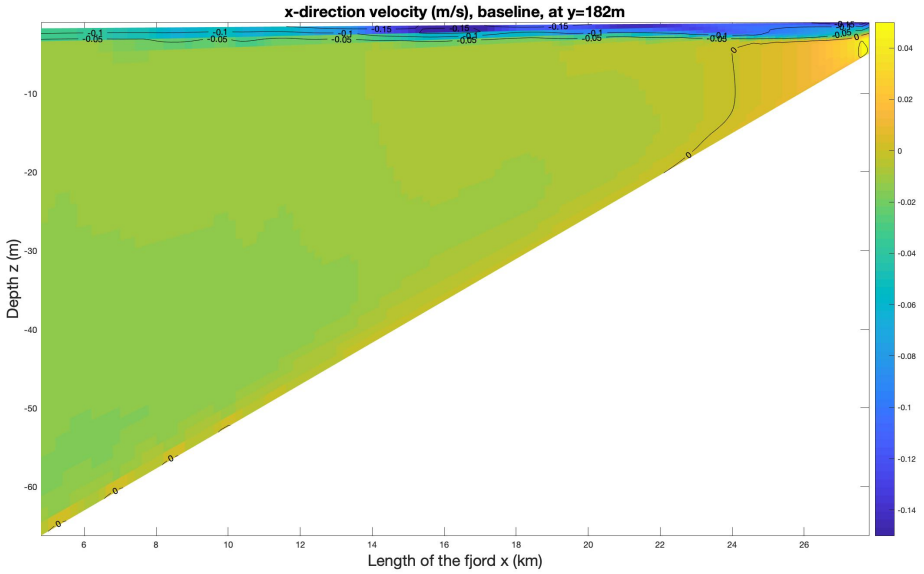

Figure 6.2: x-direction velocity (m/s) in the idealized fjord, baseline, at y=182m

6.2 Salinity and velocity sensitivities to a decrease in friction

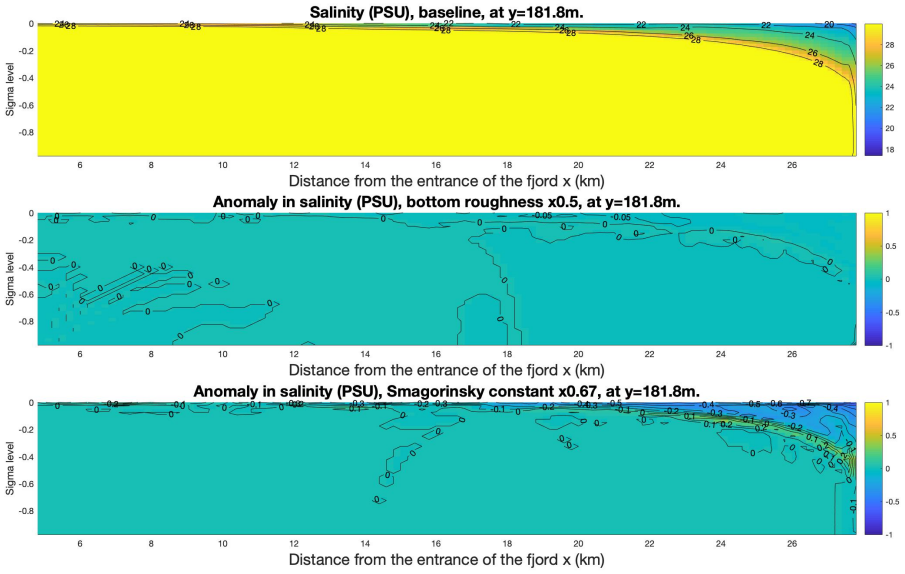

Figure 6.3: Salinity distribution sensitivity to variations in friction. The uppermost plot represents the baseline salinity distribution in the fjord. The lower three plots represent the anomaly in salinity distribution for a decrease in bottom friction, lateral viscosity coefficient (respectively).

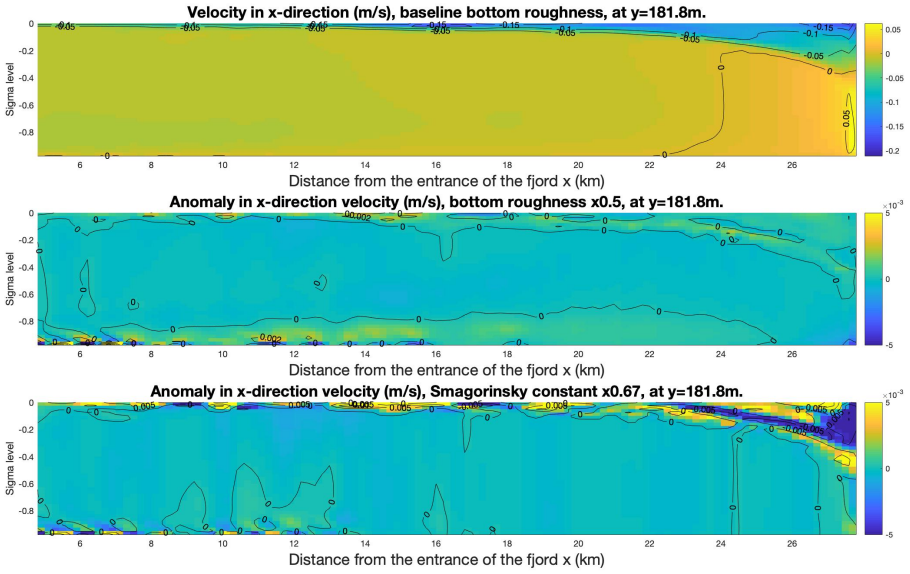

Figure 6.4: x-direction velocity sensitivity to variations in friction. The uppermost plot represents the baseline velocity distribution in the fjord. The lower three plots represent the anomaly in salinity distribution for a decrease in bottom friction, lateral viscosity coefficient (respectively).

6.3 On the influence of tides in the idealized fjord

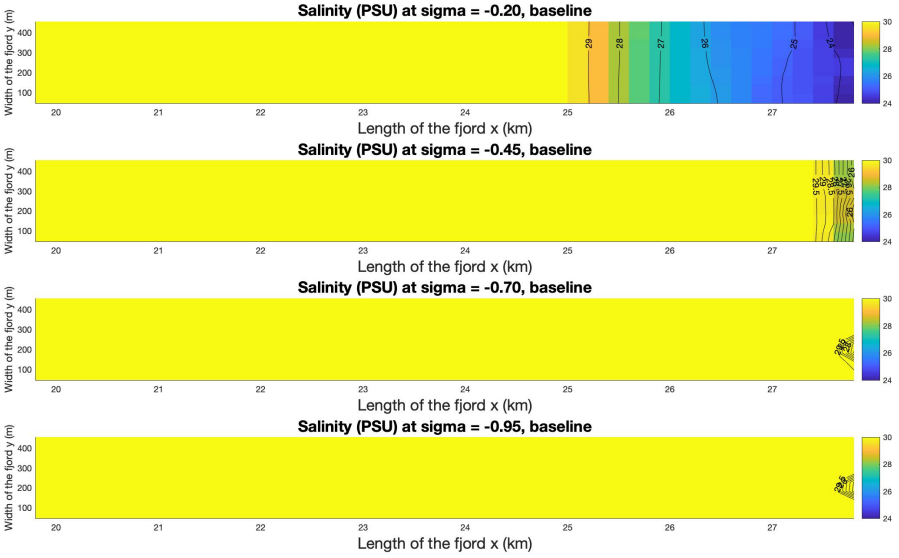

Figure 6.5: Salinity distribution for the baseline run, with tides. The uppermost plot represents the water just below the surface. The lower plots correspond to increasing depth, along sigma level.

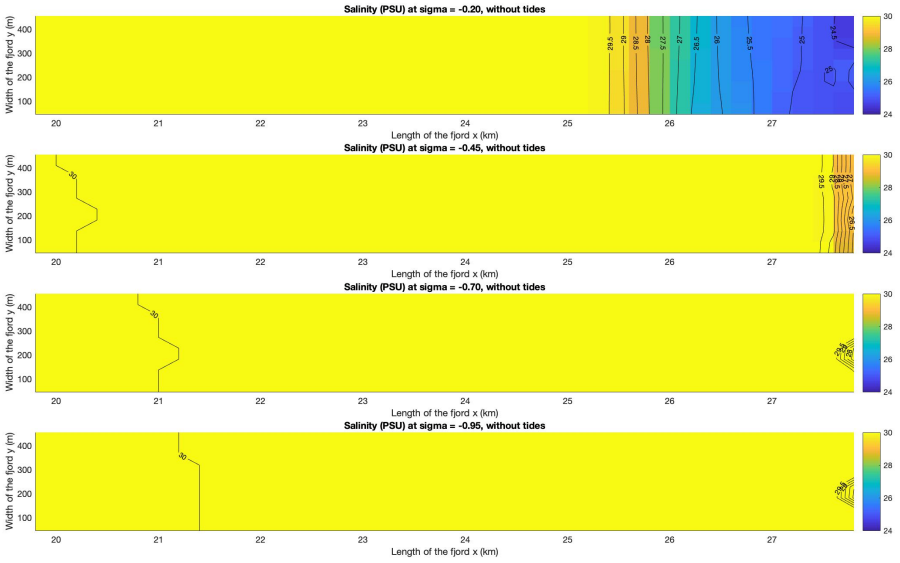

Figure 6.6: Salinity distribution for the baseline run, without tides. The uppermost plot represents the water just below the surface. The lower plots correspond to increasing depth, along sigma level.

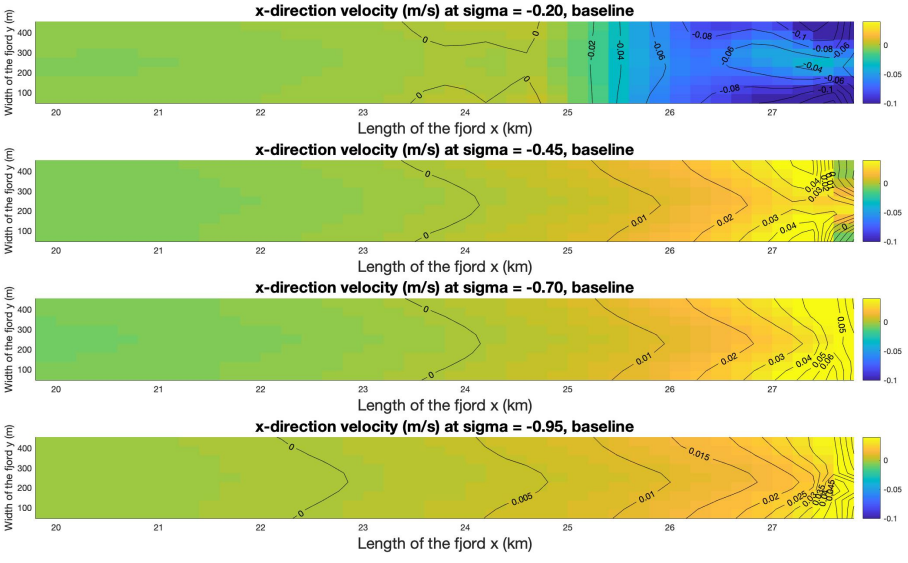

Figure 6.7: x-direction velocity for the baseline run, with tides. The uppermost plot represents the water just below the surface. The lower plots correspond to increasing depth, along sigma level.

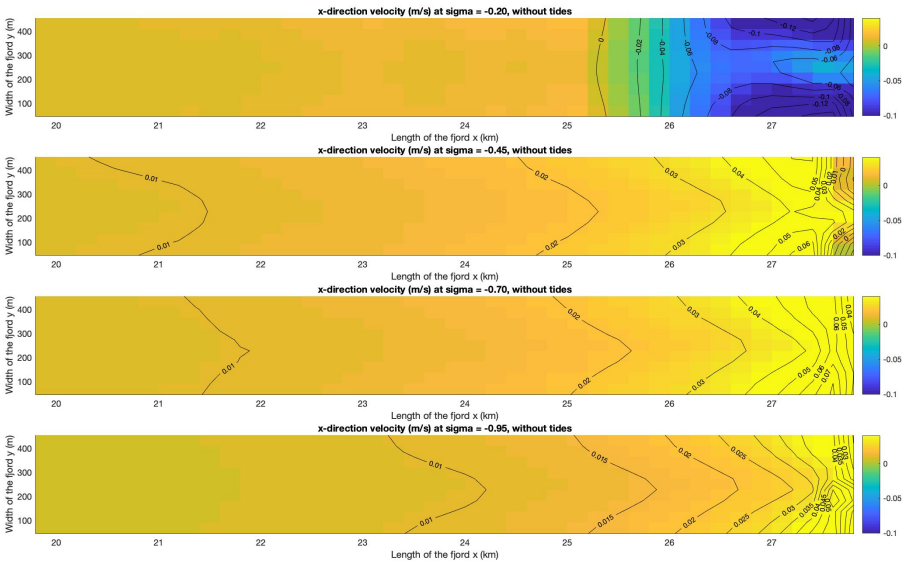

Figure 6.8: x-direction velocity for the baseline run, without tides. The uppermost plot represents the water just below the surface. The lower plots correspond to increasing depth, along sigma level.

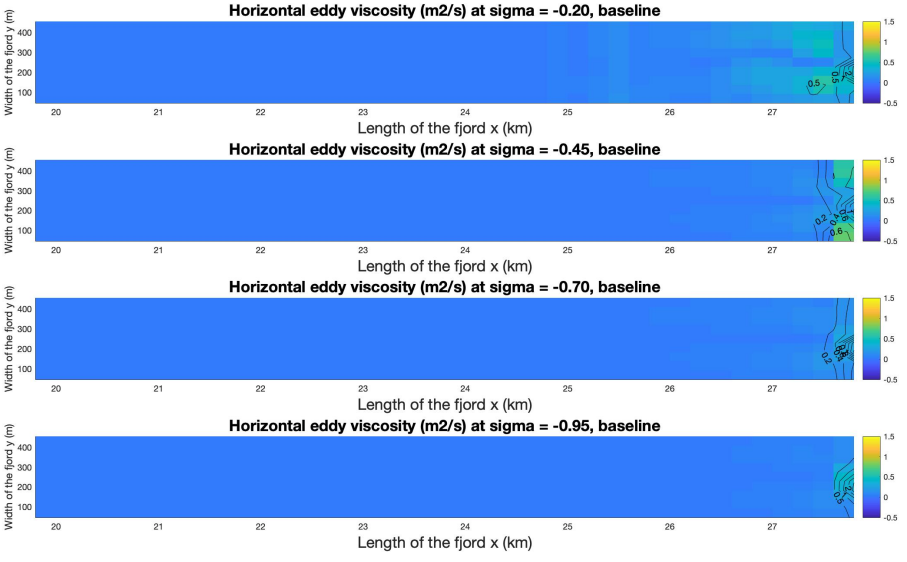

Figure 6.9: Horizontal viscosity for the baseline run, with tides. The uppermost plot represents the water just below the surface. The lower plots correspond to increasing depth, along sigma level.

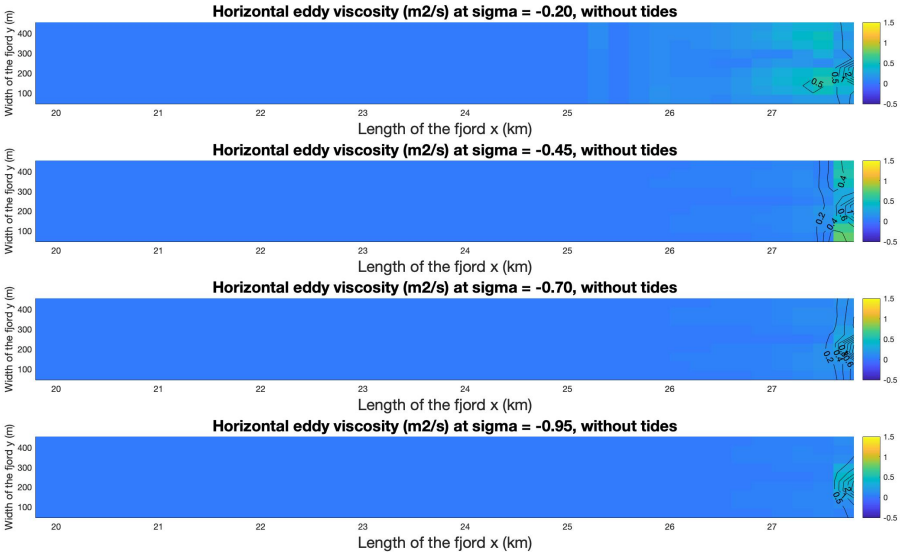

Figure 6.10: Horizontal viscosity for the baseline run, without tides. The uppermost plot represents the water just below the surface. The lower plots correspond to increasing depth, along sigma level.